A WIND TUNNEL INVESTIGATION OF CIRCULAR AND STRAKED CYLINDERS IN TRANSONIC CROSS FLOW

JOHN M. MACHA

a report from the Texas A&M RESEARCH FOUNDATION

College Station, Texas

Prepared for

National Aeronautics and Space Administration
Ames Research Center
Moffett Field, CA.

Under Grant NSG-2123

TAMU Report 3318-76-01
November 1976

A WIND TUNNEL INVESTIGATION OF CIRCULAR AND STRAKED CYLINDERS IN TRANSONIC CROSS FLOW

JOHN M. MACHA

TAMU Report 3318-76-01
Texas A&M Research Foundation
College Station, Texas 77843

November 1976

Prepared for

NASA Ames Research Center
Moffett Field, CA.

Under Grant NSG-2123

Abstract

Pressure distributions around circular and circular/strake cylinders were measured in a wind tunnel at Mach numbers from 0.6 to 1.2 with Reynolds number independently variable from 0.1×10^6 to 1.0×10^6. The local pressures are integrated over the cylinder surface to determine the variation of drag coefficient with both Mach number and Reynolds number. Effects of tunnel blockage are evaluated by comparing results from circular cylinders of various diameters at common Mach and Reynolds number conditions. Compressibility effects are concluded to be responsible for a slight reduction of the drag coefficient near Mach 0.7. Drag increases with strake height, presumably approaching a maximum drag corresponding to a flat plate configuration.

1.0 Introduction

The static longitudinal forces and moments for aircraft and missiles at high angles of attack can be predicted by semi-empirical techniques which combine the lift force derived from potential flow theory with a force attributed to the separation of the viscous cross flow.[1] The viscous term must be evaluated from an experimentally determined cross flow drag coefficient. Since the aircraft or missile in a cross flow appears as a two-dimensional bluff body (with application of slender body theory), the drag coefficient may be a function of both cross flow Mach number and Reynolds number.

The drag coefficient is also a function of the particular shape of the vehicle cross section. Consequently, drag coefficients of entire families of elliptic, polygonal, and wind-body combination cross-sectional shapes must be determined from wind tunnel tests. As an alternative, a method has been proposed which computes the drag coefficient of a body of non-circular cross section based on an equivalent circular section.[2]

Numerous wind tunnel tests have been conducted to measure the drag coefficients of circular and non-circular bluff cross sections. Most of these have been in either of two Mach number ranges: (1) the low subsonic where compressibility effects can be ignored and blockage effects are minimal; or (2) fully supersonic flow. It is well known that at low Mach numbers ($M \leq .25$) the drag coefficient is dominated by Reynolds number effects. However, the actual values are influenced by stream turbulence, surface roughness and wall interference so that considerable scatter exists in the data. For Mach numbers greater than 2.0 the available data indicate little dependence on Reynolds number and the agreement among various

investigators is good. Reference 1 contains an extensive bibliography of existing circular cylinder drag data.

Until now, few attempts had been made to measure the drag coefficient of bluff cylinders through the transonic range. Wind tunnel tests at Mach numbers approaching transonic have yielding drag coefficients influenced to an unknown extent by wall interference.[3,4] A flight test program[5] using sounding rockets with circular cylinders extended from the tail fins produced drag coefficients for Mach numbers from 0.5 to 1.3 but with no way to separate the effects of Mach number and Reynolds number.

The purpose of the wind tunnel investigation reported here was to determine drag coefficients for circular and circular/strake cross sections through the transonic speed range. The application is to provide the empirical data required to predict the aerodynamics of flight vehicles at high angles of attack. This research was supported by Grant NSG-2123 from the NASA Ames Research Center.

2.0 Experimental arrangement

The experiment was carried out in the Two-by-Two-Foot (61cm x 61cm) Transonic Wind Tunnel at the NASA Ames Research Center. The facility is a closed-return, variable density tunnel equipped with an adjustable, flexible-wall nozzle and a slotted test section. Stagnation pressure can be varied from 0.16 to 3.0 atmospheres, yielding a Reynolds number range from 0.5×10^6 to 8.7×10^6 per foot with Mach number independently variable from 0.2 to 1.4.

For these two-dimensional tests the slotted sidewalls were replaced with solid walls incorporating circular, optical glass windows through which

the ends of the models were mounted (See Figure 1). The slotted sections remained in the floor and ceiling. A calibrated drive system was attached to the window frame to rotate the window-model combination. Shadowgraph and schlieren techniques were used extensively to visualize shock formations and the shedding of vortices.

3.0 Models

Seven models were used during the course of the experiment. Four were circular in cross section with diameters of 1.91, 2.54, 3.81, and 5.0 centimeters. Three others of 2.54cm diameter were modified by the addition of a thin strake running the length of the model and are identified in this report by the ratio of the strake height to the diameter -- s/d = 1.2, 1.55, and 2.0. Figure 2 is a sketch of the model cross sections. The straked cylinders were tested with the strakes normal to the tunnel flow. All of the models were machined from 303 stainless steel stock to a smooth finish but not highly polished. The roughness height was 1.6×10^{-4}cm measured in the axial direction. Each circular cylinder contained nine surface pressure orifices separated by 40 degrees of circumference and staggered laterally about the center four inches of the model. The straked models, which could not utilize the rotation capability of the installation, were provided with 17 orifices distributed around the circumference. In addition, orifices were located on the forward and rearward faces of the strakes -- a total of eight orifices on the s/d = 1.55 and 2.0 models and five on the s/d = 1.2 model. The orifices were connected by tubing to pressure transducers which, in turn, provided electrical signals that were digitized and recorded.

4.0 Computation of drag coefficnets

Surface pressures were recorded in the form of pressure coefficents, $C_p = \frac{p-p_\infty}{\frac{1}{2}\rho_\infty V_\infty^2}$, at each of the nine orifices as the circular models were rotated in increments of three degrees. The subscript "∞" refers to the static pressure, density, and velocity of the undisturbed flow ahead of the model. Components of the pressure coefficients parallel to the free stream direction were then summed over the circumference to yield a drag coefficient, C_D, based on the projected model area normal to the flow. Drag coefficients for the straked cylinders were computed in the same manner except that the models could not be rotated.

5.0 Results and discussion

Figure 3 is a matrix of the models and conditions tested. Reynolds number is based on the diameter of each of the circular models, and in the case of the straked models, on the 2.54cm diameter.

Tables 1 and 2 summarize the uncorrected drag coefficients computed for the circular and straked cylinders, respectively.

5.1 Blockage effects. The interference of wind tunnel walls with the flow past a bluff body is always of concern and this concern is amplified as the test Mach number approaches unity. For this reason circular cylinders of diameters of 1.91, 2.54, 3.81, and 5.08cm corresponding to solid blockages of 3.1, 4.2, 6.2, and 8.4 percent, respectively, of the tunnel cross section were tested at identical Mach and Reynolds conditions. The resulting drag coefficients are plotted as a function of Mach number and model diameter-to-tunnel height ratio, d/h, in Figures 4a and 4b.

Blockage effects are apparently eliminated by the slotted floor and ceiling at Mach numbers up to 0.6. From Mach = 0.6 to 0.9 the higher blockages increasingly alter the drag coefficient; the measured C_D is greater than it would be if the tunnel walls were not present. At Mach 1.0 blockage effects are extreme. At supersonic Mach numbers the effects are moderate and appear to lessen with increased Mach number. Also, at Mach 1.0 and greater the effect of blockage on the drag coefficient has reversed compared to the subsonic cases; the computed C_D's are less than the uninterfered-with values would be.

Use has been made of Figure 4b to obtain crudely corrected drag coefficients for Mach numbers of 1.0 and greater by extrapolating the curve for a particular Mach number back to zero blockage. The resulting corrected C_D's for Mach numbers equal to 1.0, 1.1, and 1.2 are about 1.90, 1.70, and 1.60, respectively.

Figure 5 shows that at Mach = 1.0 the effect of blockage is to alter the location of separation, and consequently, the value of the pressure coefficient over the aft portion of the cylinder. Figure 6 presents the variation with blockage of pressure coefficients averaged over the separated flow region of the cylinder for Mach numbers of 1.0 and higher. Since the pressure coefficients for the Mach 1.0 curves in Figure 5 are essentially constant over the rear of the cylinder, the pressure distribution could reasonably be modified to reflect the extrapolated value of about -1.25 from Figure 6. When this is done the resulting computed drag coefficient is 1.92, in agreement with Figure 4b.

5.2 Mach number effects. Earlier wind tunnel investigations by Knowler and Pruden[3] and Matt[4] and flight tests by Welsh[5] showed a first maximum in the drag coefficient of circular cylinders at a Mach number of about 0.65 which preceeds the absolute maximum near Mach 1.0. The dashed curve in Figure 7 shows the results of Welsh for a cylinder with a fineness ratio of 60. In those experiments, Reynolds number changed with Mach number so that either could be responsible for the drag reduction. In many cases the reduction coincided with a Reynolds number in the low speed "critical" range. In the present tests, Mach number was varied with Reynolds number held constant and the maximum still occurred. The observations pertaining to this drag reduction which will now be discussed must be due entirely to compressibility effects.

From results of Gowen and Perkins[6], at Mach numbers from 0.3 to 0.7 where the final separation is laminar, the point of boundary layer separation moves forward on the front side of the cylinder and the suction pressure over the back side increases. This, combined with the increased stagnation pressure, raises the drag coefficient from about 1.2 to 1.6. Schlieren photographs from the present tests indicate that as Mach number increases above 0.7 the separation point shifts rearward and pressure distributions show that the base pressure becomes less negative. For instance, from Figure 8a for Mach equal to 0.9 separation is at about 85 degrees and the value of the base pressure coefficient is about -0.9. The result is a reduction of the drag coefficient as seen in Figure 7. At a Mach number of 1.0 (Figure 8b) separation occurs aft of 100 degrees but the suction has increased to a corrected C_p of about -1.25 and the corrected drag coefficient is 1.92.

As Mach number increases supersonically the location of separation remains fixed at about 110 degrees but the base pressure steadily increases causing lower drag coefficients. This trend continues to higher supersonic Mach numbers where Gowen and Perkins found a base C_p of -0.1 and a drag coefficient of 1.35 for Mach equal to 2.9. The range of C_D indicated by the symbols for the present test in Figure 7 at subsonic Mach numbers is due to variation with Reynolds number. For Mach numbers of 1.0 and greater the vertical bars indicate the estimated uncertainty in the corrected values.

While it is reasonable to assume that at Mach numbers approaching unity compressiblity effects should begin to dominate the flow around the cylinder, the mechanism which fixes the separation prematurely compared to a low speed turbulent separation at the same Reynolds number is still unclear. Schlieren photographs in Figures 9 show the development of shock waves on a circular cylinder and on its wake and the shedding of vortices alternately from one side and then the other. At Mach numbers of 0.6 and 0.7 nearly normal shocks are situated on the shoulders of the cylinder coincident with the point of flow separation. At Mach numbers of 0.8 and greater these disturbances become more and more oblique and a normal shock of increasing strength develops on the wake. The arc in the first quadrant and near circular spot above the models are faults in the windows. Also unexplained is the behavior of the suction pressures on the back side of the cylinders illustrated in Figures 8a and 8b. At lower Mach numbers the pressures become more negative proceeding from the point of separation toward the rear stagnation point. For Mach numbers of 0.9 and greater the pressures remain constant with circumferential angle in this region.

5.3 Reynolds number effects. The decreasing dependence of drag coefficient on Reynolds number as Mach number approaches unity is illustrated in Figure 10. Only at the lowest test Mach number of 0.6 does a trend exist after allowance for the blockage effect. The pressure distributions in Figure 11 show that the increase in drag coefficient as Reynolds number increases to about 0.7×10^6 is the result of later separation at greater suction pressures. This behavior is just the opposite of that at low speeds where delayed separation results in less negative base pressures. As Reynolds increases above 0.7×10^6 the drag coefficient decreases slightly due to improved pressure recovery.

Also indicated in Figure 11 for a Mach number of 0.6 is the critical pressure coefficient, C_p^*, at which the local flow becomes sonic. At the higher Reynolds numbers the supersonic region begins about 65 degrees from the front stagnation but the flow remains completely subsonic at the lowest Reynolds number. Locally supersonic flow existed for all tests at Mach numbers of 0.7 and greater.

5.4 Roughness effects. Figure 12 shows the effect on pressure distributions of 0.005cm spherical roughness applied uniformly around the circumference of the 2.54cm diameter model. At Mach numbers up to 0.9 the roughness produces more negative peak pressures followed by greater recoveries resulting in decreases in the drag coefficients. At Mach 1.0 and higher the pressure distributions are unaffected by the addition of roughness.

5.5 Straked models. Figure 13 is a pressure distribution typical of those measured on the straked cylinders. Even at the smallest strake height-to-cylinder diameter ratio, s/d, of 1.2 the strake edge is the dividing point between the positive and the suction pressures.

It was apparent from the tests on the circular models that computed drag coefficients of the straked models would be significantly affected by tunnel blockage near Mach 1.0. Consequently, "corrected" values for the drag coefficients are estimated from the circular results. Figure 14 illustrates the application of a quadratic equation to the circular cylinder data at Mach = 1.0 for the ratio of the corrected to uncorrected drag coefficients. The value of the drag coefficient at zero blockage is arbitrarily chosen as 1.90. Assuming that the variation of measured drag with solid blockage of the straked models grossly follows the variation for the circular cylinders, the quadratic equation is applied to the measured drag coefficients for the straked models. The blockage ratios for the s/d = 1.2 and 1.55 models are 0.05 and 0.065, respectively. It is realized that this is a questionable assumption since the primary effect of blockage on the circular cylinder is to change the location of separation (recall Figure 5) while for the straked cylinders, separation must remain fixed at the strake edge. Nevertheless, corrected C_D's with an estimated uncertainty less than ± 10% are plotted in Figure 15 for Mach 1.0, together with uncorrected values for the rest of the Mach number range. In each case the drag coefficient is based on the plan area of the strake. The drag coefficient versus Mach number curves in Figure 15 possess the same first maximum as Figure 7 for the circular models. In addition, there appears to be an increasing Reynolds number influence on the Mach number at which the maximum occurs as the s/d ratio is increased. Comparison of wake widths in Figure 16 determined from shadowgraphs of the s/d = 1.55 model also produces

trends with both Reynolds number and Mach number. The width, b, is taken at one diameter downstream from the model and is nondimensionalized by the strake height, s. Figures 17a and 17b present the trend in drag coefficient in going from a circular cylinder toward a flat plate configuration for the various Mach numbers tested. A schlieren photograph of the s/d = 1.55 straked model is reproduced as Figure 18.

6.0 Concluding remarks

A series of two-dimensional circular and circular/strake cylinders has been tested in a transonic wind tunnel. As Mach number increases through transonic, the pressure drag increases until about Mach 0.7, remains constant or decreases slightly to Mach 0.9, increases significantly near Mach 1.0 and decreases with increasing supersonic Mach numbers. The leveling-off of the drag variation prior to the major drag rise near Mach 1.0 is concluded to be a compressibility effect and not a Reynolds number effect as speculated in previous investigations. The effect of increasing Reynolds number on the circular cylinders is to slightly increase the drag but this effect diminishes as Mach number approaches unity. Artificial surface roughness has little effect on the drag coefficient at high subsonic Mach numbers and no effect for Mach = 1.0 and higher. The drag of a straked cylinder increases with strake height-to-cylinder diameter ratio, apparently approaching a maximum corresponding to a flat plate configuration.

7.0 References

1. Jorgensen, L.H., "Prediction of static aerodynamic characteristics for space-shuttle-like and other bodies at angles of attack from 0 degrees to 180 degrees," NASA TN D-6996, January, 1973.

2. Jorgensen, L.H., "A method for estimating static aerodynamic characteristics for slender bodies of circular and noncircular cross-section alone and with lifting surfaces at angles of attack from 0° to 90°," NASA TN D-7228, April 1973.

3. Knowler, A.E. and F.W. Pruden, "On the drag of circular cylinders at high speeds," R&M No. 1933, British A.R.C., 1944.

4. Matt, H., Forschg. Ber. Nr. 1825 der ZWB, 1943. Results also in Von A. Naumann and F. Pfeiffer, "Uber die Grenzschichtablosung am Zylinder bei hohen Geschwindigkeiten," Advances in Aeronautical Sciences, ed. by Th. von Karman, Vol. 3, pp. 185-206, 1962.

5. Welsh, C.J., "The drag of finite length cylinders determined from flight tests at high Reynolds numbers for a Mach numbers range from 0.5 to 1.3," NACA TN 2491, June 1973.

6. Gowen, F.E. and E.W. Perkins, "Drag of circular cylinders for a wide range of Reynolds numbers and Mach Numbers," NACA TN 2960, June 1953.

Mach No.	d[a] = 1.91		d = 2.54		d = 3.81		d = 5.08		d = 2.54 +Roughness	
	R_d[b]	C_D	R_d	C_D	R_d	C_D	R_d	C_D	R_d	C_D
0.6	.12	1.46	.33	1.47	.33	1.44	.33	1.47	.16	1.36
	.19	1.46	.42	1.49	.44	1.53	.83	1.55	.42	1.41
	.28	1.44	.50	1.58	.56	1.58				
	.33	1.44			.62	1.62				
					.69	1.62				
					.75	1.58				
					.86	1.52				
0.65							.92	1.53		
							1.0	1.52		
0.7	.12	1.54	.17	1.52	.33	1.58	.34	1.61	.17	1.48
	.19	1.54	.33	1.52	.41	1.58	.82	1.68	.42	1.47
	.28	1.56	.42	1.55	.56	1.60	.92	1.63		
	.33	1.57	.50	1.56	.63	1.59				
					.69	1.61				
					.75	1.59				
0.8	.13	1.57	.33	1.51	.33	1.58	.33	1.62	.17	1.46
	.19	1.53	.42	1.53	.44	1.58	.67	1.59	.48	1.46
	.28	1.52	.49	1.54	.56	1.59	.75	1.59		
	.33	1.54			.61	1.60	.83	1.61		
0.9	.12	1.47	.25	1.57	.33	1.54			.17	1.58
	.19	1.45	.33	1.57	.44	1.55			.33	1.53
	.28	1.52								
1.0	.13	1.79	.25	1.72	.33	1.44	.33	1.33		
	.19	1.77	.33	1.72	.44	1.43				
	.28	1.78								
1.06									.33	1.68
1.10	.13	1.67	.17	1.64					.17	1.65
	.19	1.67								
1.20	.13	1.58	.17	1.56					.17	1.57
	.19	1.59	.25	1.56						

[a] Cylinder diameter in cm [b] Reynolds number x 10^{-6}

Table 1. Uncorrected drag coefficients - circular models.

Mach No.	s/d = 1.2		s/d = 1.55		s/d = 2.0	
	R_d[a]	C_D	R_d	C_D	R_d	C_D
0.6	.17	1.80	.17	1.88	.17	2.09
	.50	1.84	.33	1.90	.33	2.07
			.50	1.92	.42	2.08
0.7	.17	1.80	.17	1.88	.17	2.11
	.50	1.79	.33	1.90	.33	2.10
			.50	1.84		
0.8	.17	1.68	.17	1.84	.17	1.96
			.33	1.87	.33	2.04
0.9	.33	1.72	.17	1.77		
1.0	.17	1.83	.17	1.80		
1.05	.17	1.84				

[a] Reynolds number x 10^{-6}

Table 2. Uncorrected drag coefficients - straked models.

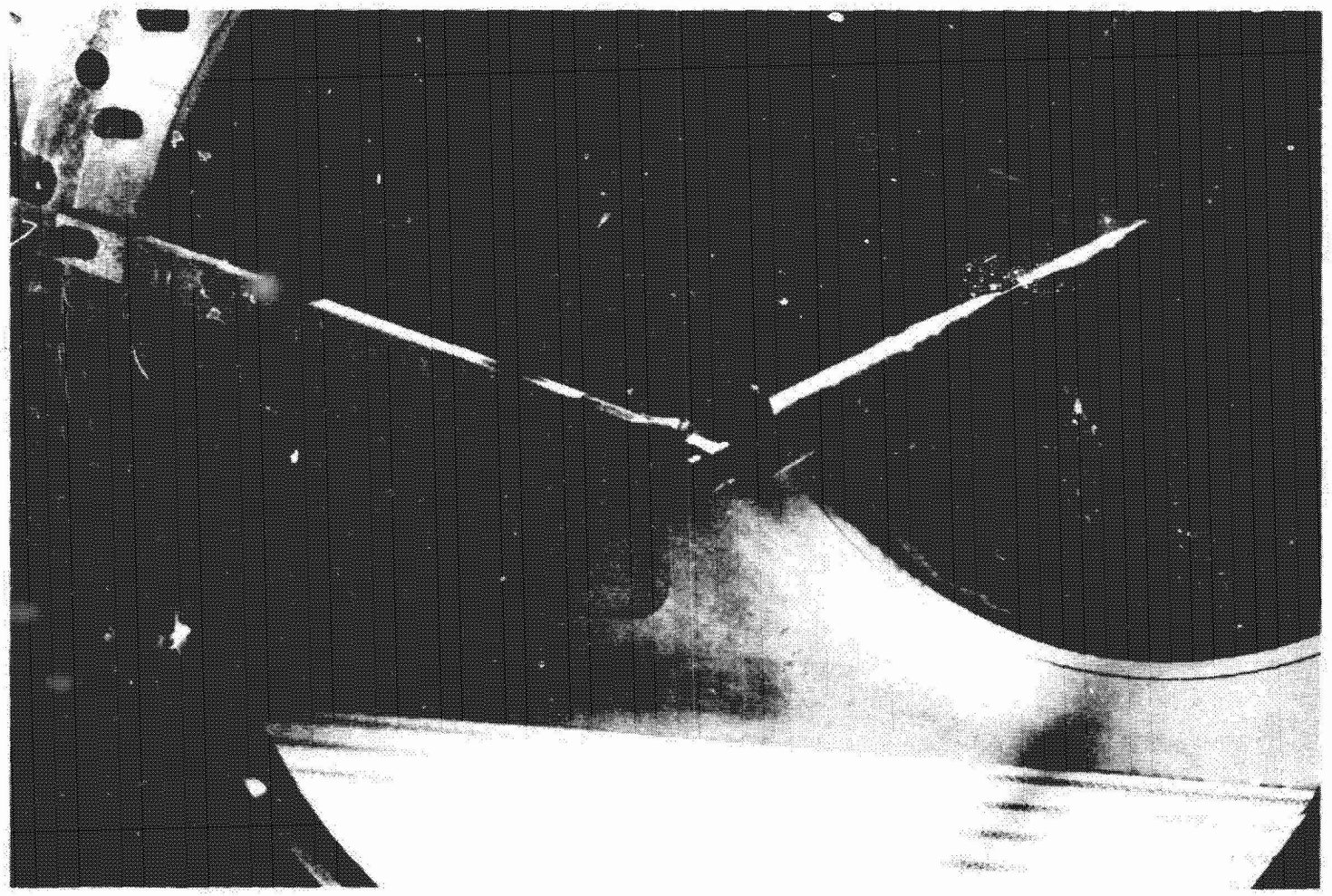

Figure 1. 2.54cm circular model installed in wind tunnel test section.

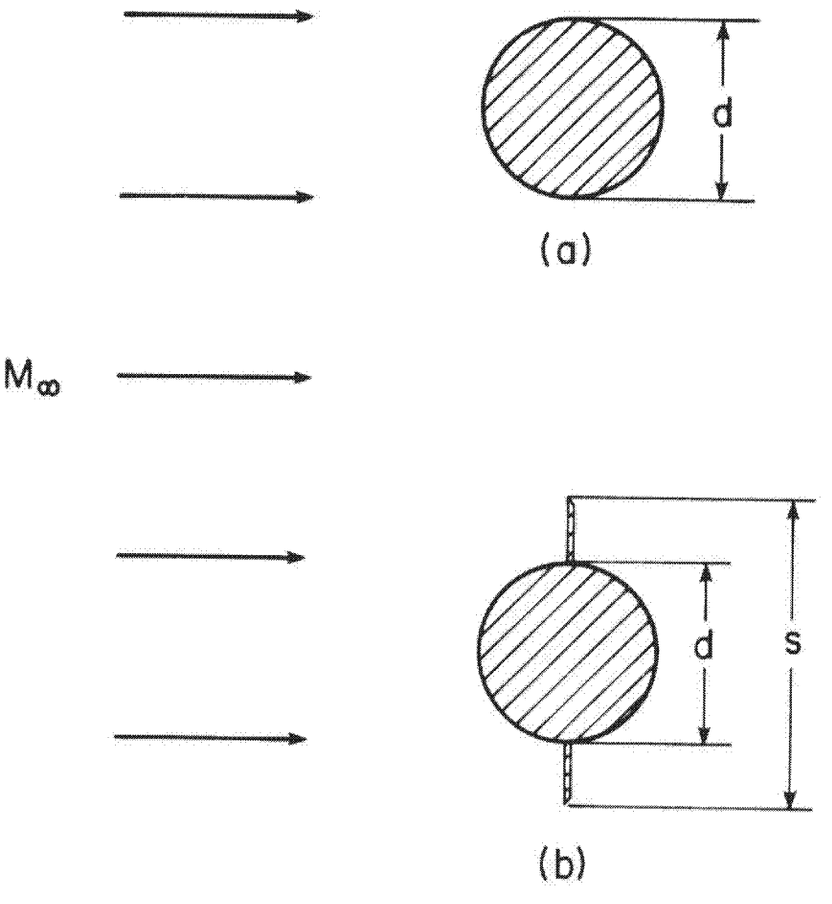

Figure 2. Cross sections of cylindrical models : (a) circular; (b) circular/strake.

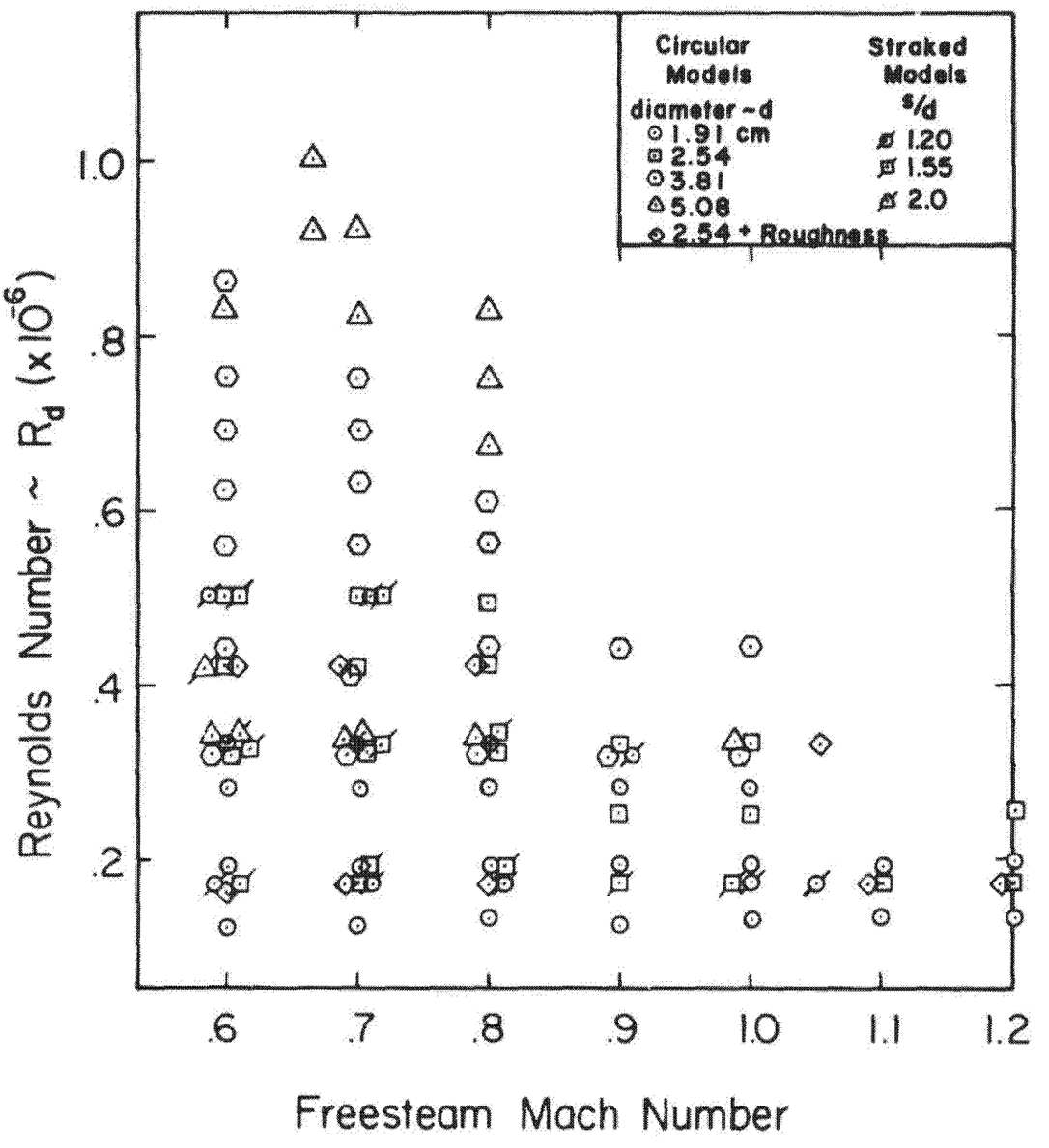

Figure 3. Matrix of models and test conditions.

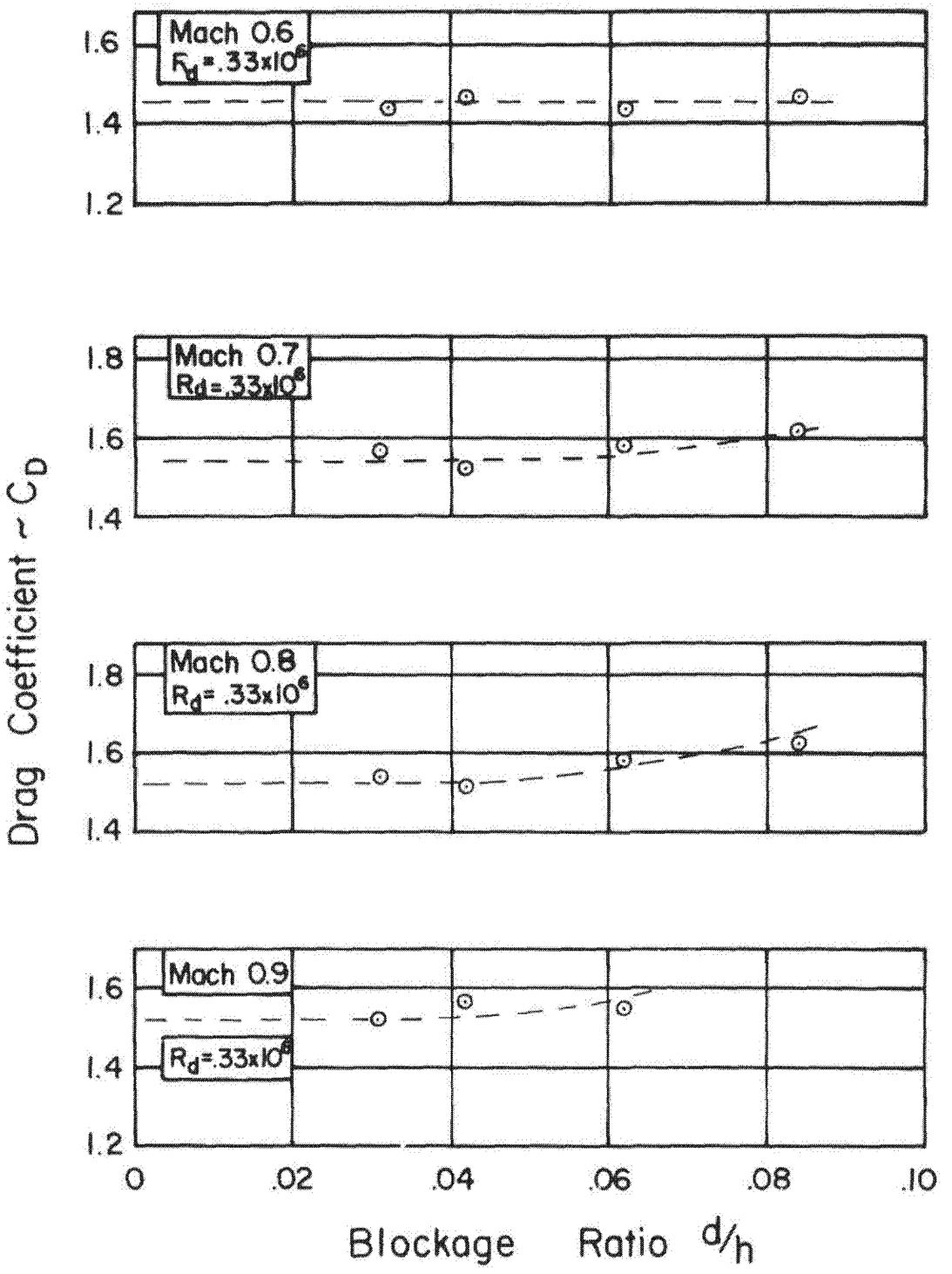

Figure 4a. Effect of tunnel blockage on the computed drag coefficients of the circular models; Mach number = 0.6 to 0.9.

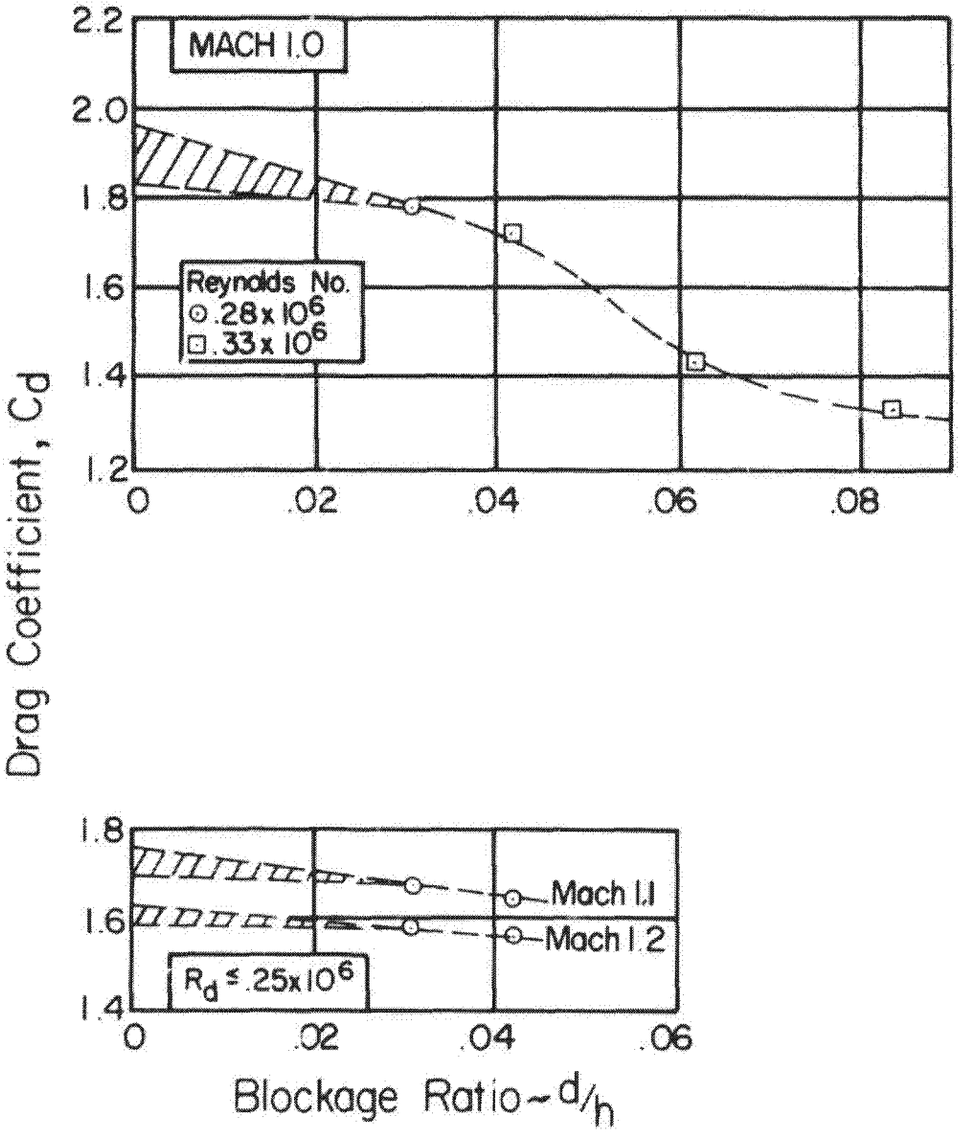

Figure 4b. As in Figure 4a except Mach number = 1.0 to 1.2.

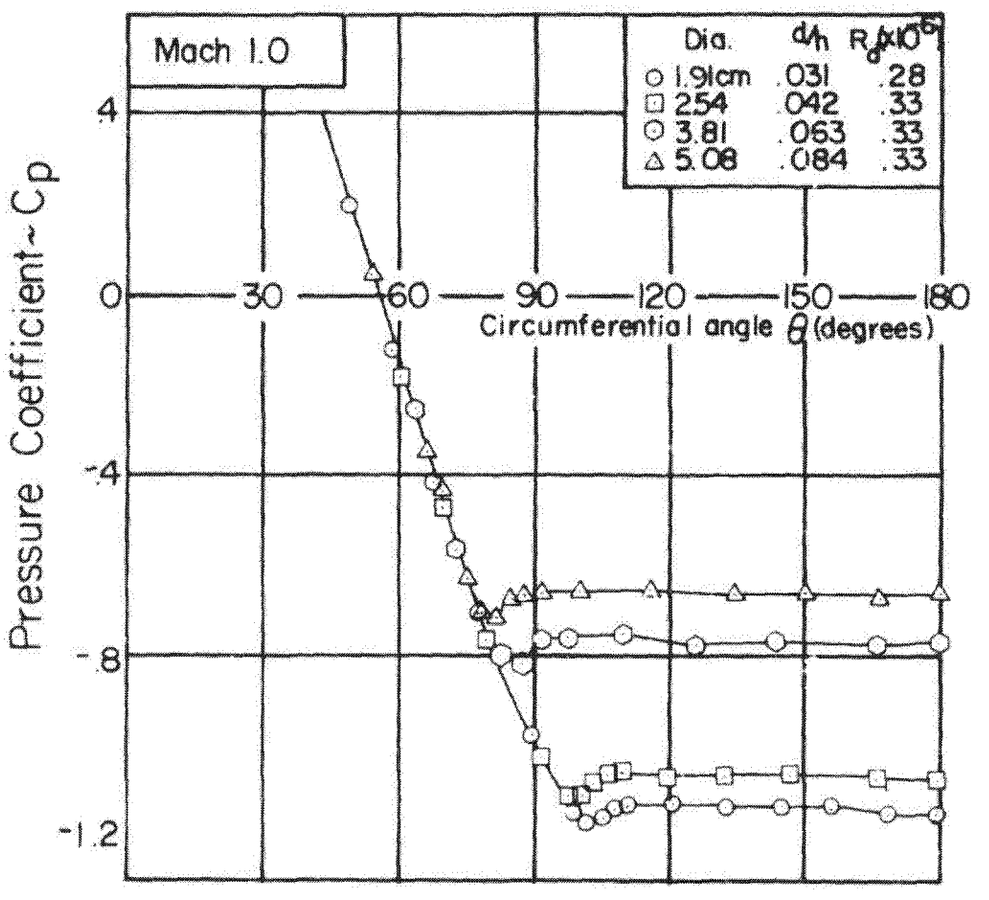

Figure 5. The effect of tunnel blockage on the circular cylinder pressure distribution at Mach = 1.0.

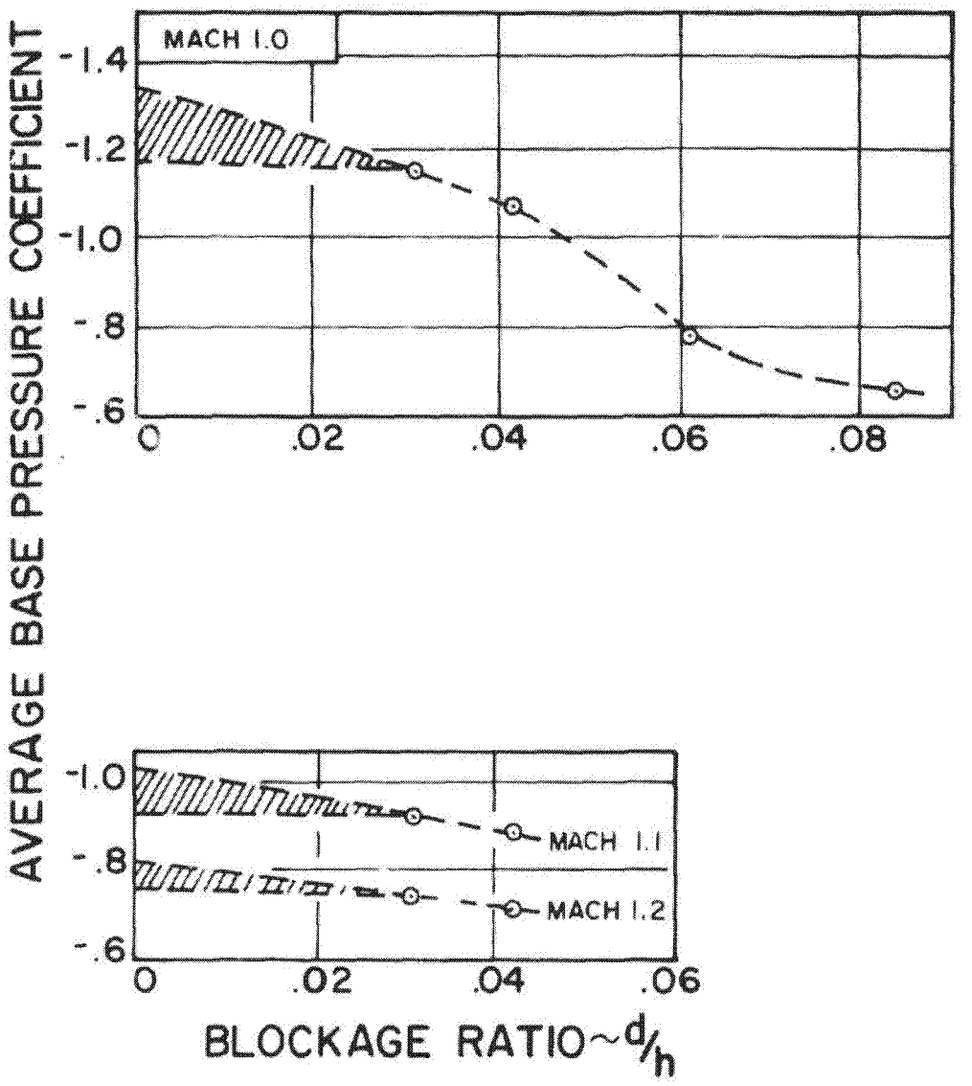

Figure 6. The effect of tunnel blockage on the averaged base pressure coefficients of the circular models.

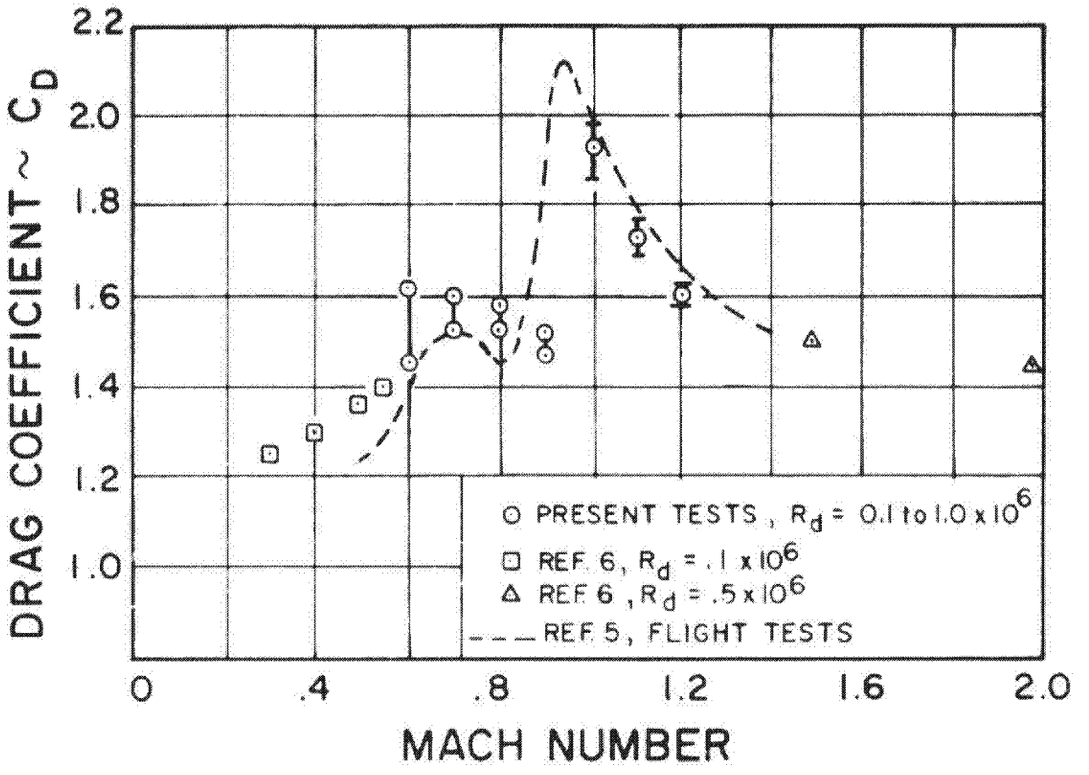

Figure 7. The variation of circular cylinder drag with Mach number.

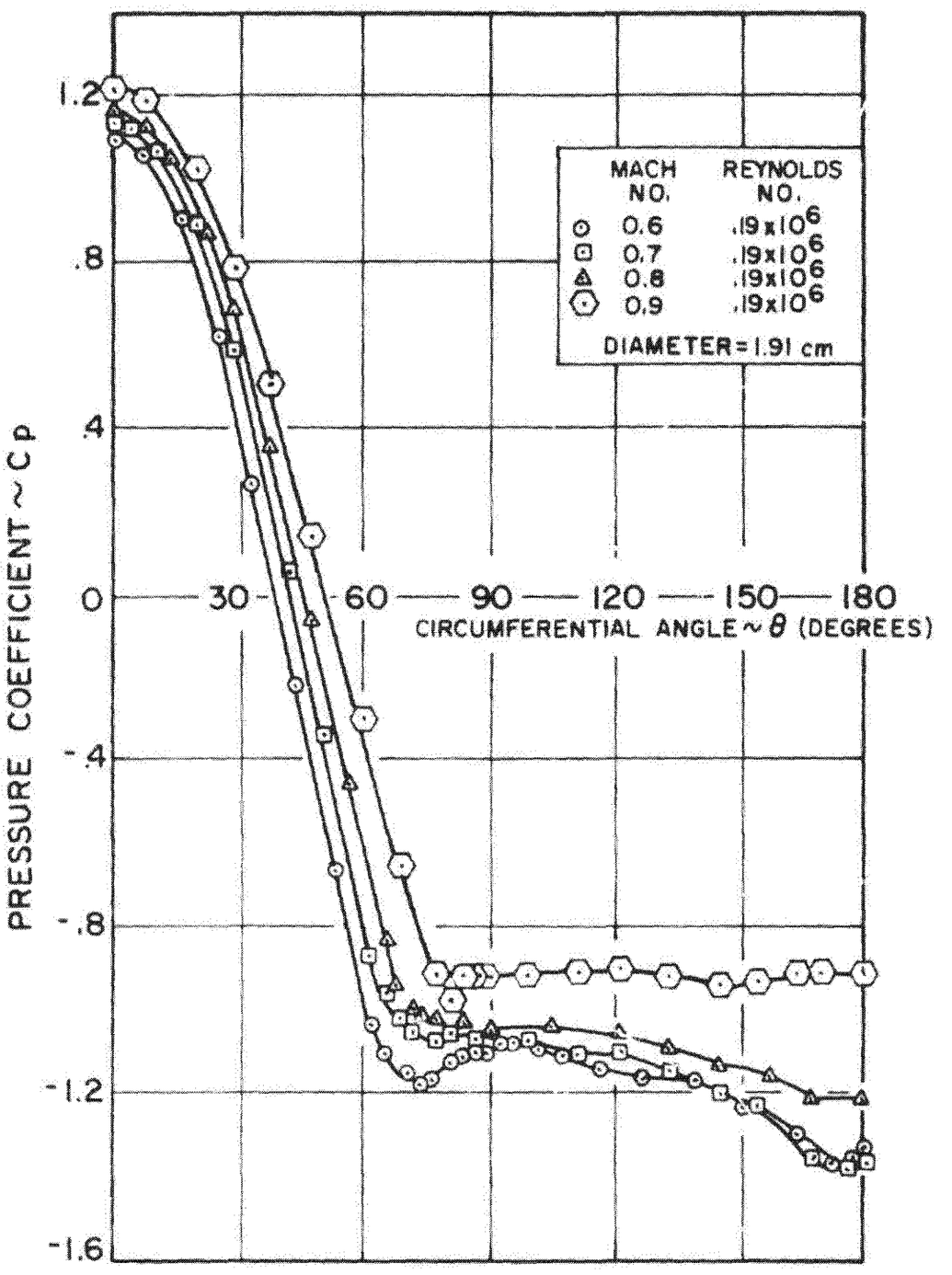

Figure 8a. Circular cylinder pressure distributions; Mach number = 0.6 to 0.9.

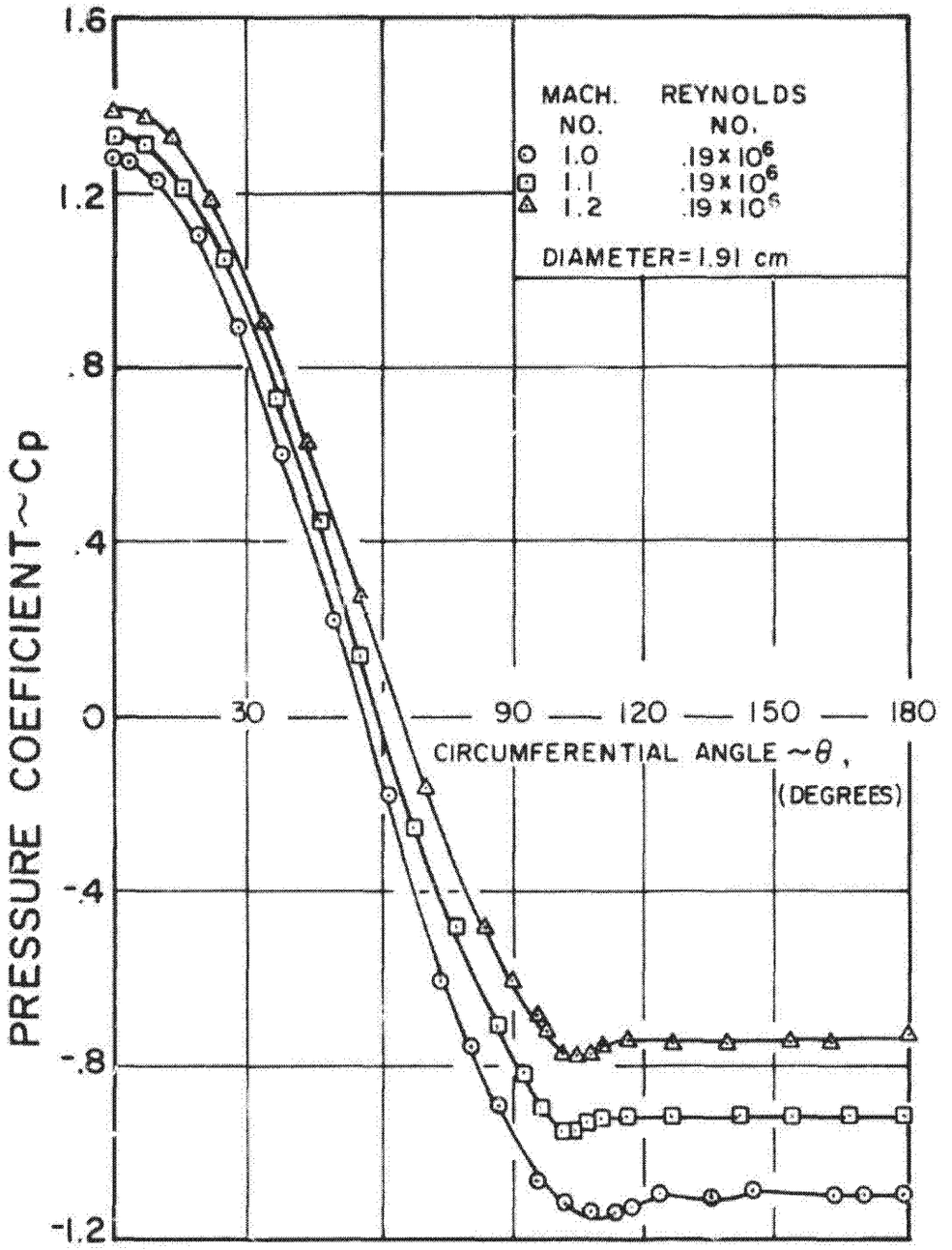

Figure 8b. As in Figure 8a except Mach number = 1.0 to 1.2.

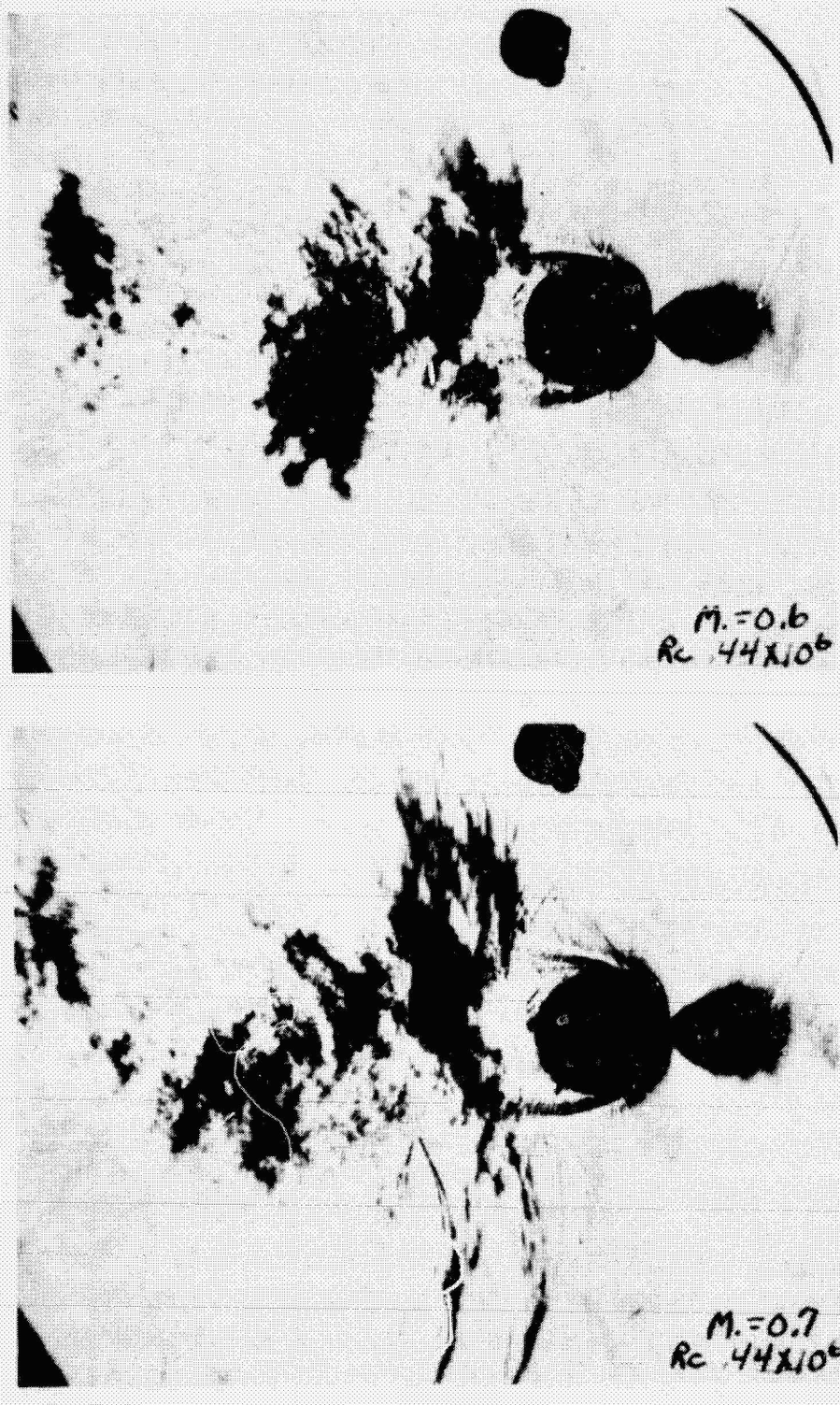

Figure 9. Schlieren photographs of the d = 3.81cm circular model. $R_d = 0.44 \times 10^6$. Upper: Mach = 0.6; lower: Mach = 0.7.

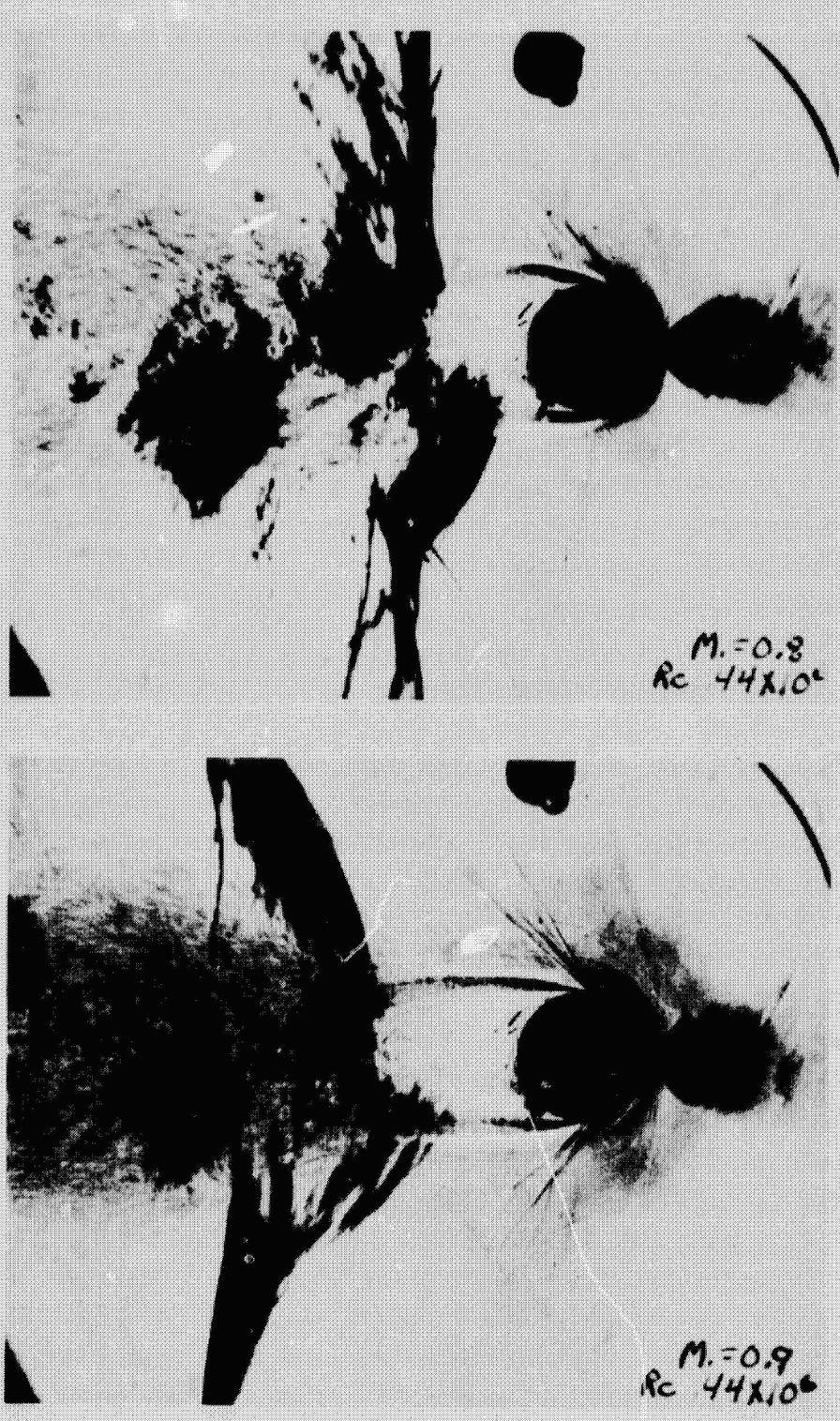

Figure 9 continued. Upper: Mach = 0.8; lower: Mach = 0.9.

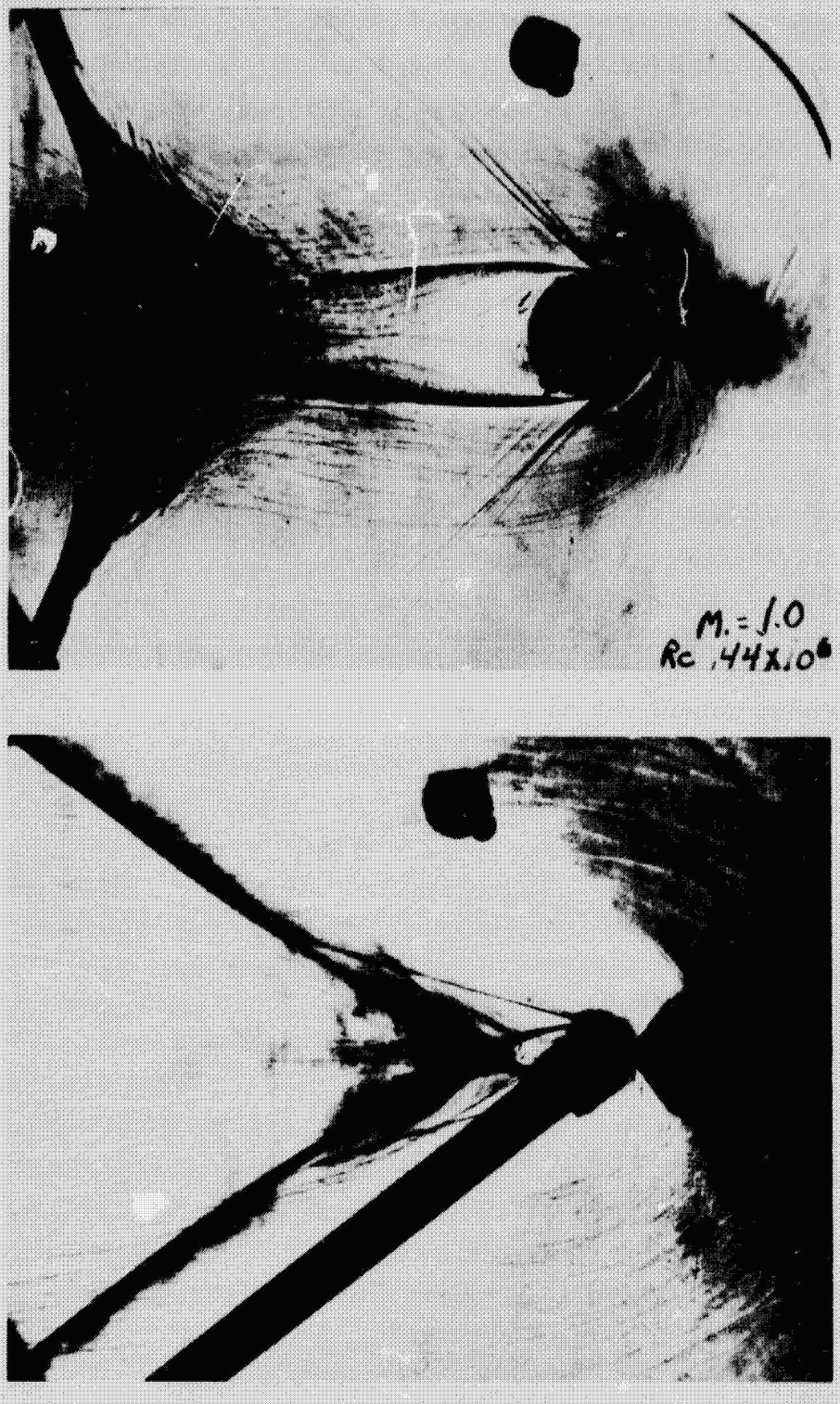

Figure 9 concluded. Upper: Mach = 1.0; lower: d = 1.91cm, $R_d = 0.19 \times 10^6$, Mach = 1.2.

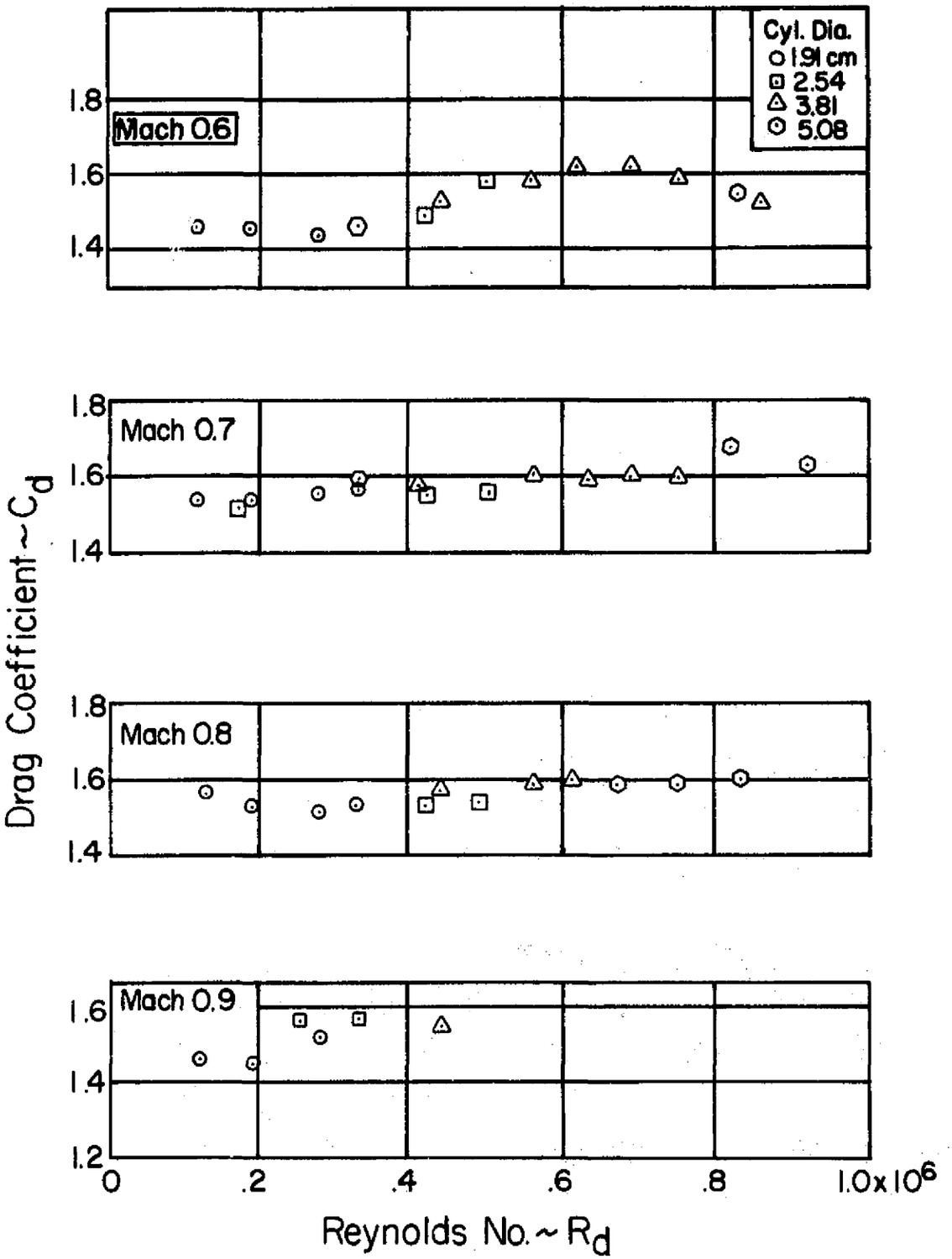

Figure 10. The variation of circular cylinder drag coefficient with Reynolds number.

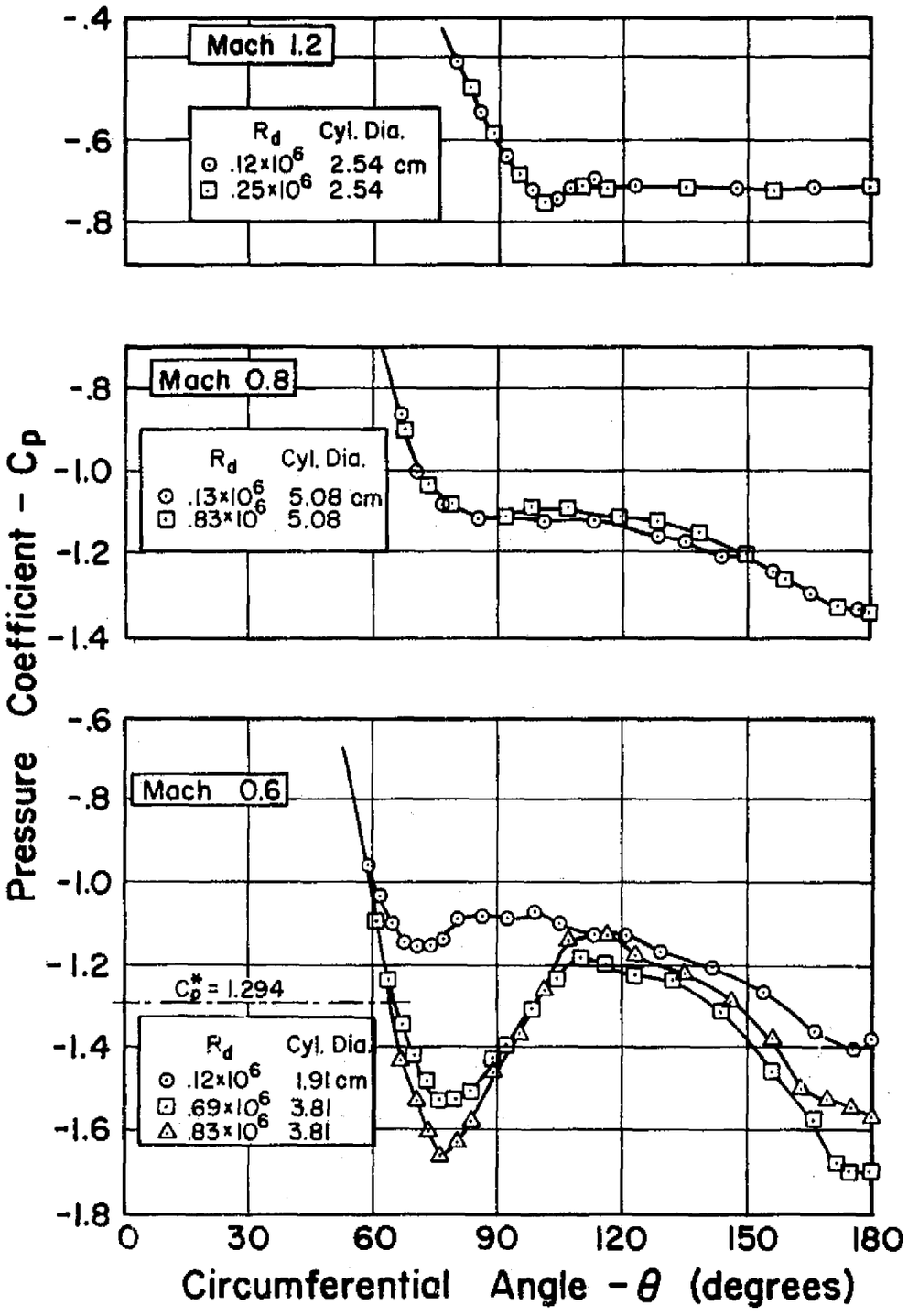

Figure 11. The effect of Reynolds number on circular cylinder pressure distributions.

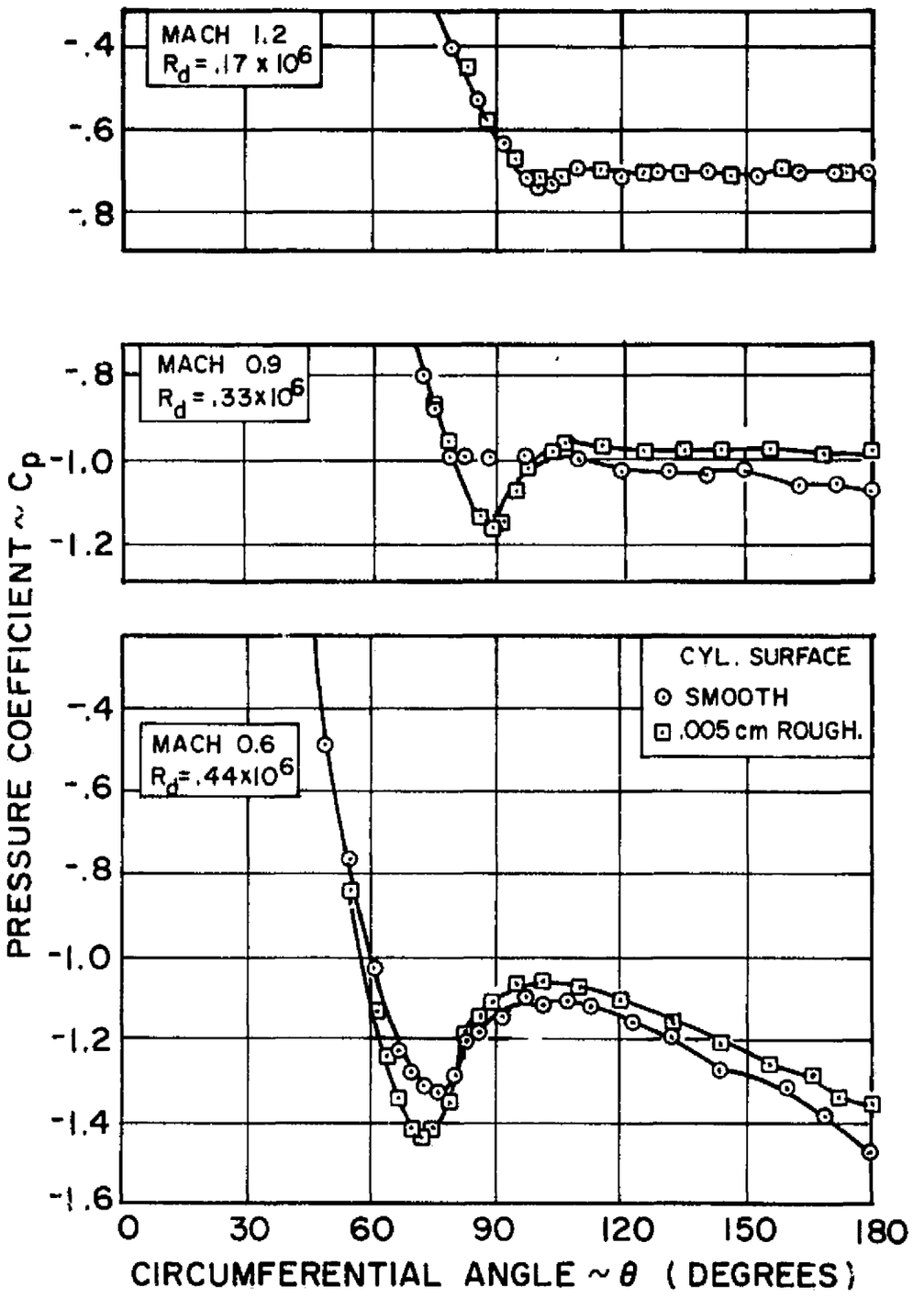

Figure 12. The effect of artificial surface roughness on pressure distributions for the d = 2.54 cm circular model.

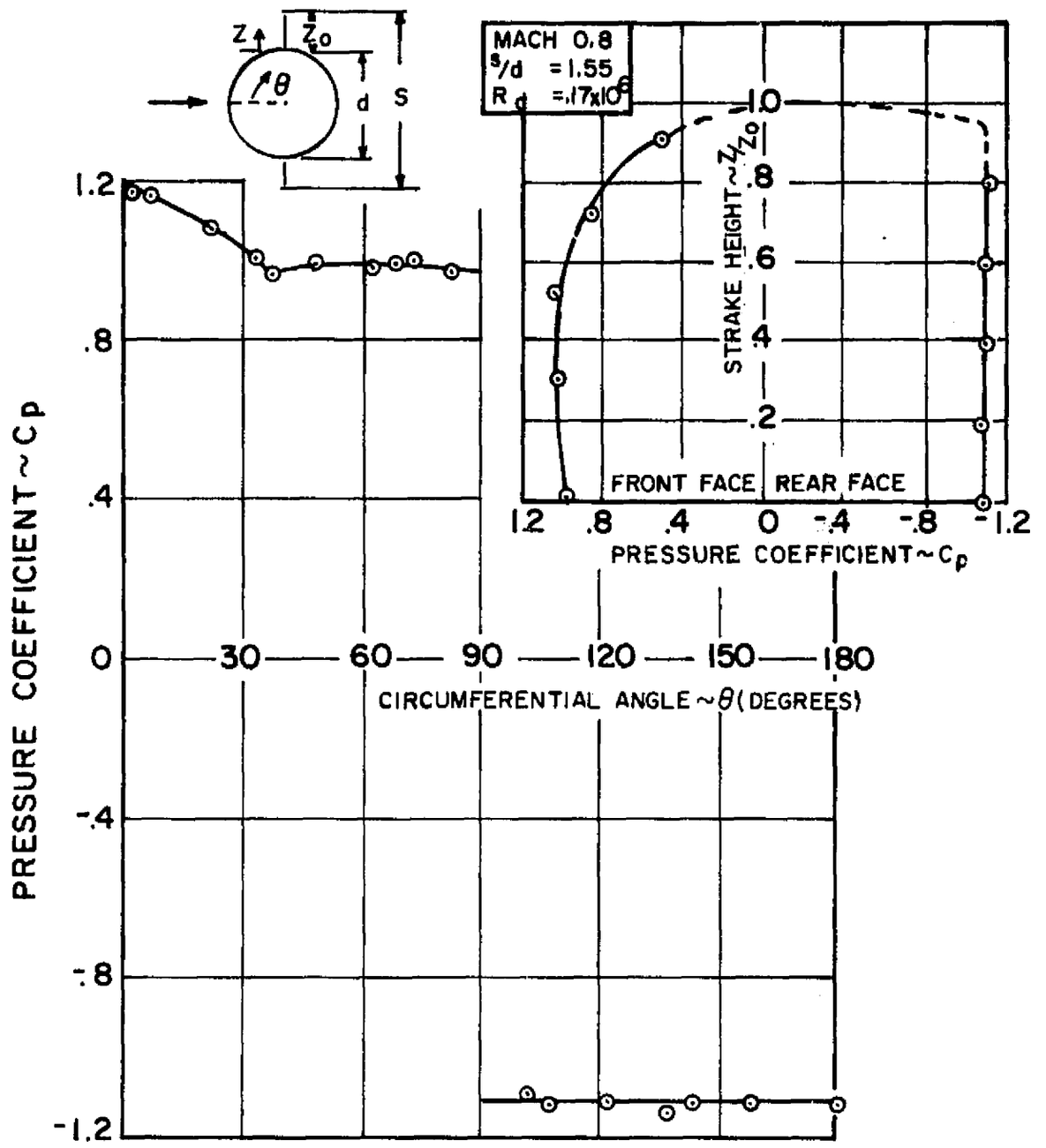

Figure 13. A pressure distribution typical of those measured for the circular/strake models.

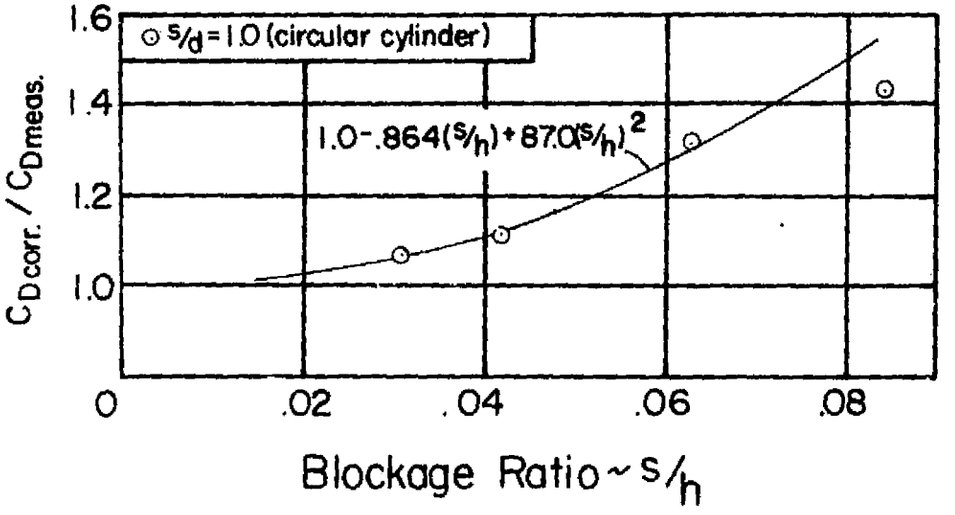

Figure 14. Curve fit to the effect of tunnel blockage on the computed drag coefficient at Mach = 1.0.

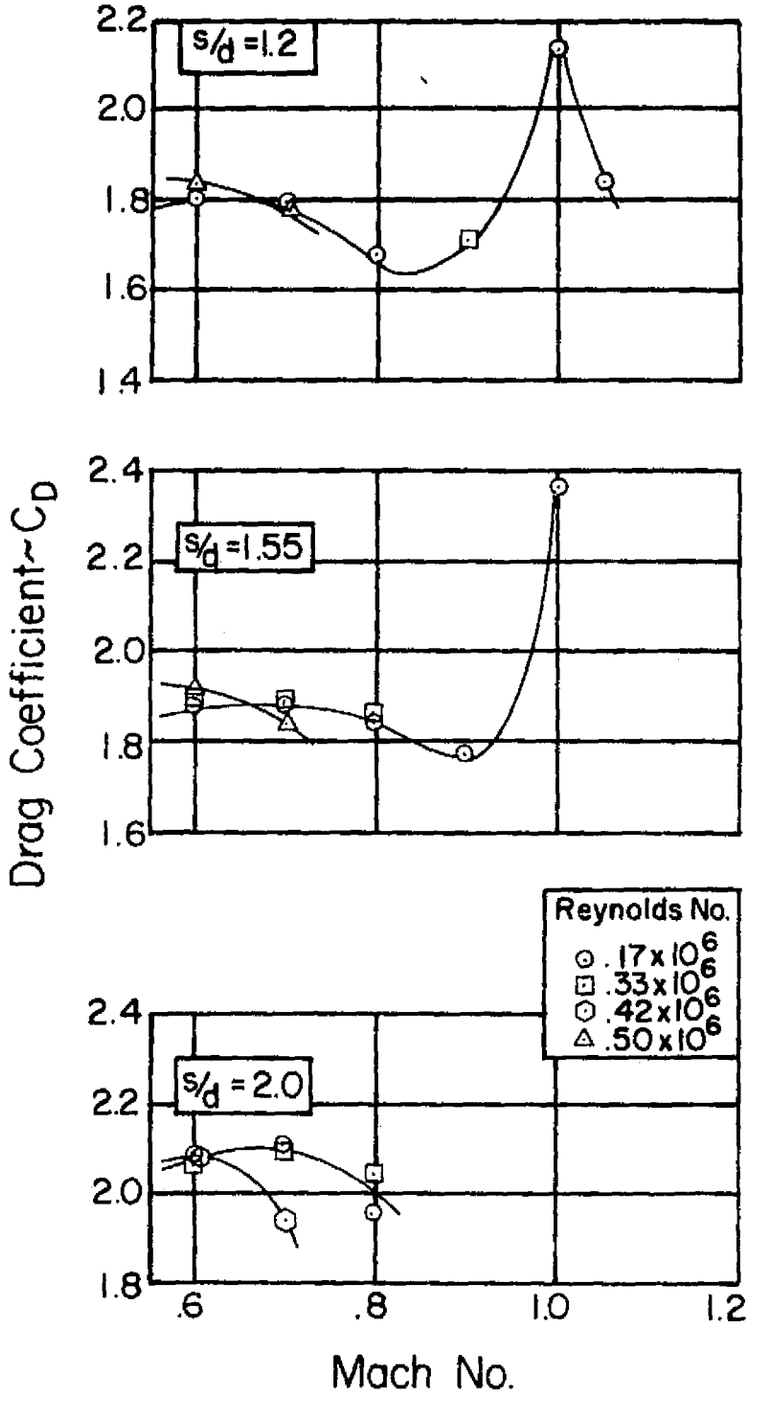

Figure 15. The variation of drag with Mach number for the straked cylinders.

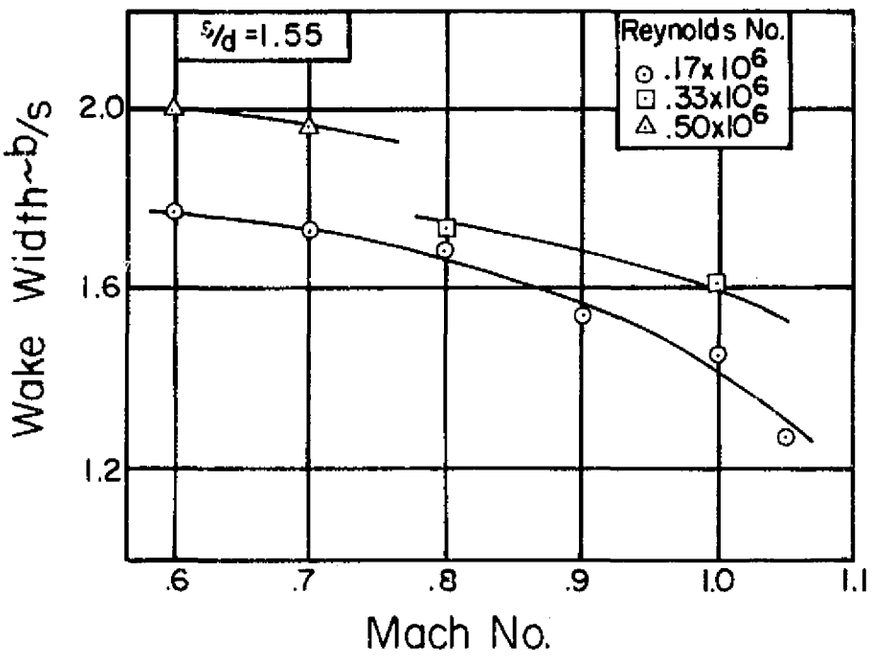

Figure 16. The variation of the non-dimensionalized wake width of the straked cylinders with Mach number and Reynolds number.

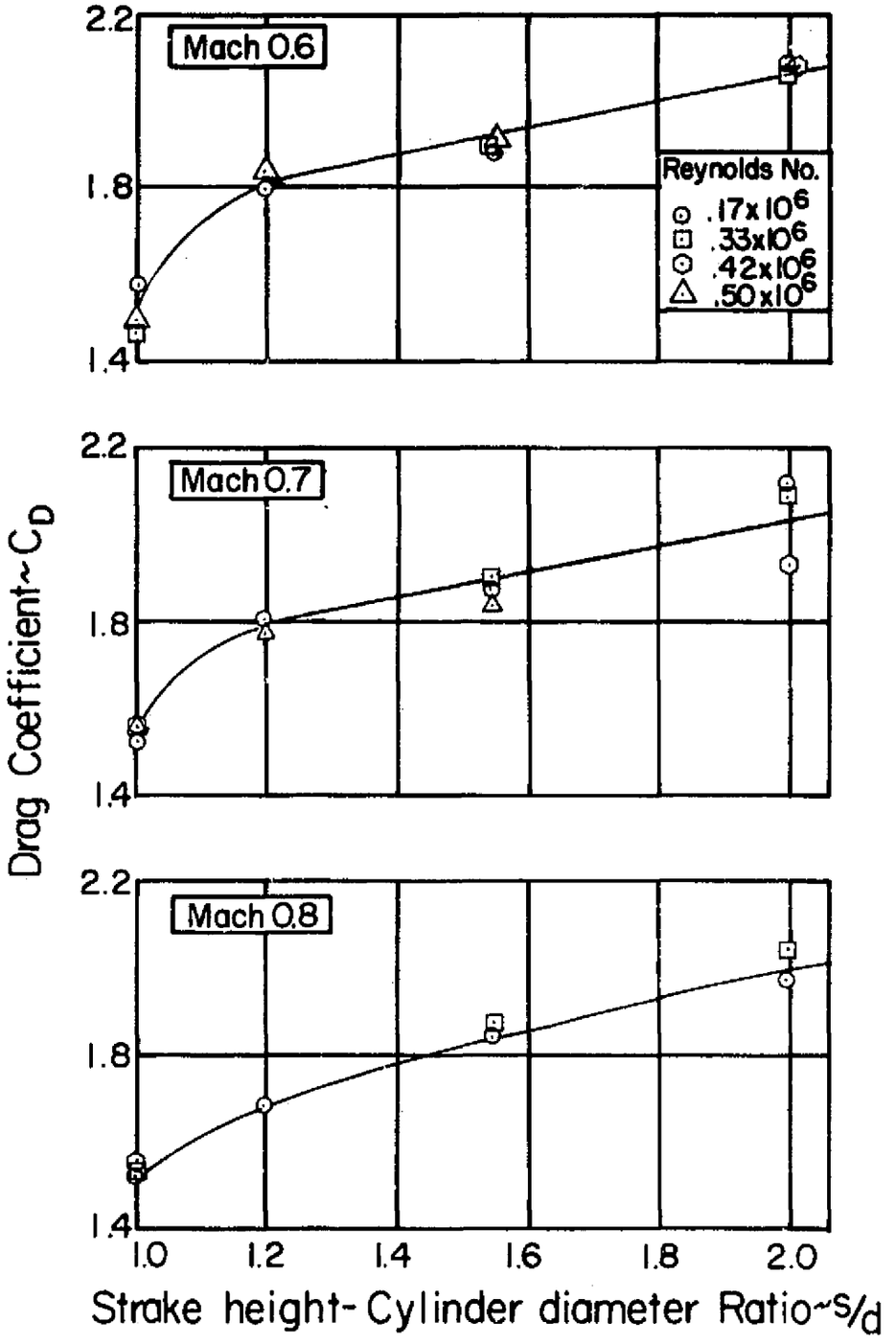

Figure 17a. The variation of drag coefficient with strake height-to-cylinder diameter ratio; Mach number = 0.6 to 0.8.

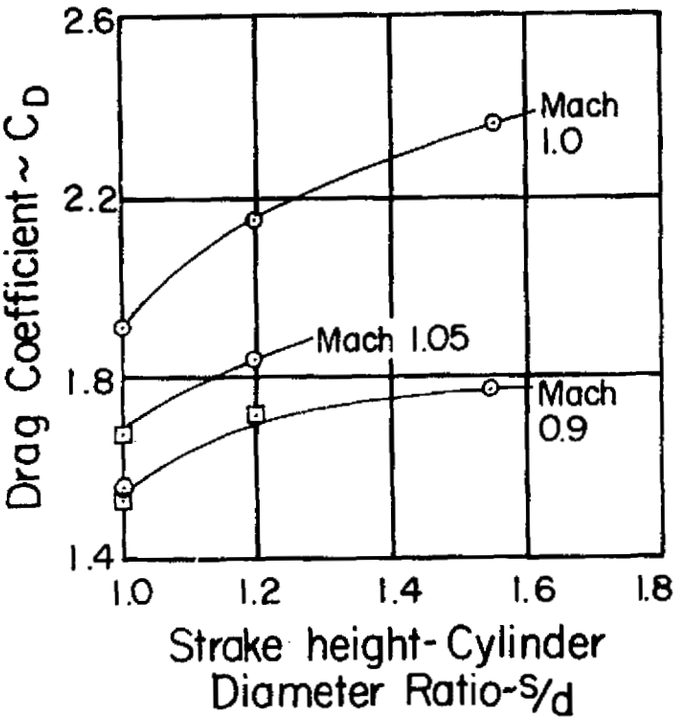

Figure 17b. As in Figure 17a except Mach number = 0.9 to 1.05.

Figure 18. Schlieren photograph of the s/d = 1.55 straked model; $R_d = 0.33 \times 10^6$, Mach = 1.0.